A Study on the Influences of Processing Parameters on the Growth of Oxide Nanorod Arrays by Sol Electrophoretic Deposition

S.J. LIMMER*, T.P. CHOU AND G.Z. CAO

Department of Materials Science and Engineering, University of Washington, Seattle, WA, USA

gzcao@u.washington.edu

Abstract. Template-based sol electrophoretic deposition has been demonstrated as an attractive method for the synthesis of oxide nanorod arrays, including simple and complex oxides in the forms of amorphous, polycrystalline, and single crystal. This paper systematically studied a number of processing parameters to control nanorod growth by sol electrophoretic deposition. The influences of particle and template zeta potentials, condensation rate, deposition rate (or externally applied electric field), the presence of organic additives, and sol concentration on the growth of nanorod arrays were studied. It was found that higher zeta potential or electric field resulted in higher growth rates but less dense packing. Templates with charge opposite to that of the sol particles prevented formation of dense nanorods, sometimes resulting in nanotubes, depending on the field strength during electrophoresis. In addition, the pH of the sol and chelating additives were also varied and likely affected the deposition process by affecting the condensation reactions.

Keywords: sol electrophoresis, electrophoretic deposition, sol-gel processing, template-assisted nanorod growth, oxide nanorods, nanorod arrays

1. Introduction

The fabrication of nanostructures and nanomaterials with desired dimensions and compositions is an essential cornerstone of nanotechnology, and many synthesis techniques have been developed for the creation of nanostructured materials [1]. In the area of nanostructured materials, so-called one-dimensional nanostructures (nanorods, nanowires) have attracted large amounts of interest for their potential applications, along with the information they can provide about the influence of size and dimensionality on properties [2, 3]. Nanorods of oxide materials are particularly appealing [4], given the large number of functional properties that oxides exhibit. Thus, there is substantial interest in methods for the synthesis of oxide nanorods.

Present address: Materials Research Center, University of Missouri-Rolla, Rolla, Missouri, USA

The technique of sol electrophoretic deposition in templates provides a versatile method for forming nanorods of numerous simple and complex oxide nanorods [5–9], and while sol electrophoretic deposition has been known for some time as a technique for the formation of films, only recently has it been adapted for the formation of nanorods [10, 11]. In concept, the only requirement is that one applies an electric field to an electrostatically stabilized sol. Nanoclusters dispersed in such a sol would develop a surface charge, and a double layer structure in the vicinity of the nanoclusters would form due to a combination of electrostatic attraction, Brownian motion, and osmotic force, as depicted in Fig. 1. An externally applied electric field to such a colloidal system or sol would set the charged particles in motion in response to the electric field (Fig. 1), migrating such nanoclusters until the motion of such nanoclusters is stopped by either an electrode or other physical barrier. However, there are a number of parameters that significantly influence the

Figure 1. A schematic of the electrical double-layer surrounding a particle in a colloidal suspension that is responsible for the electrostatic stabilization of a colloid (left), and the electrophoretic motion and process involved in template-based sol electrophoretic deposition (right).

growth process, the microstructure, and the morphology of the resultant nanorod arrays. This has not been studied or reported in detail.

In this study, the influence of several of these processing parameters are reported, albeit less quantitative or less conclusive, so as to provide some general guidance to further study the synthesis of nanorod arrays by sol electrophoresis. More specifically, we attempted to vary independently each of six different parameters: particle zeta potential, template zeta potential, condensation rate, deposition rate, presence of stabilizing additives, and sol concentration. While some of these parameters are not strictly independent (concentration and deposition rate, for example), we separated the influences out as much as possible.

2.   Experimental

In much of this study, TiO_2 was used as a model system to examine the various processing parameters. Since SiO_2 sol can be either particulate or polymeric and $Pb(Zr,Ti)O_3$ (PZT) is a complex oxide, both systems were also used. The preparation of TiO_2 sol has been reported in Ref. 12, similar to the process reported previously [10, 11]. Briefly, the sols were prepared as

follows. TiO_2 sol was formed by dissolving titanium (IV) isopropoxide (97%, 30 mL) in glacial acetic acid (60 mL), followed by the addition of deionized (DI) water (30 mL). Upon the addition of water, a white precipitate instantaneously formed. However, the sol became a clear liquid after ∼5 minutes of stirring. The preparation of SiO_2 and PZT sols has been published in Reference 10. The SiO_2 sol was made by dissolving tetraethyl orthosilicate (98%, 21 mL) in a mixture of ethanol (8 mL) and DI water (3 mL). A small amount of hydrochloric acid (1N, 0.09 mL) was added to the sol to adjust the pH to ∼3 and the sol was stirred for 2 hrs at room temperature. The silica sol thus formed was rather stable, and took several weeks to gel at room temperature. The preparation of PZT sol was described in detail in Reference 20. Briefly, lead (II) acetate (24.48 g) is dissolved in glacial acetic acid (15.2 mL), heating to 110°C for ∼15 min to dehydrate the lead acetate. The sample is then allowed to cool back to room temperature. Because of the volatility of PbO, an excess amount of lead (5 mol%) is used in the fabrication of this sol. Then titanium (IV) isopropoxide (97%, 8.4 mL) and zirconium (IV) n-propoxide (70%, 14.72 mL) are mixed together for ∼10 min at room temperature, and added to the lead solution once it has cooled to room temperature. Deionized water (16 mL) is then added to initiate and

sustain hydrolysis and condensation reactions, and the sol is stirred for ~15 min at room temperature. Lastly, lactic acid (3.4 mL), glycerol (4.8 mL), and ethylene glycol (3.6 mL) are added to adjust the viscosity and stability of the sol. Such prepared sols have a concentration of about 5 vol% PZT, and are stable for several weeks at room temperature. These standard sols were occasionally modified by adjusting the concentration or pH, or by adding stabilizers, which is discussed in detail below.

Both polycarbonate (PC) and anodic alumina (AAM) templates, consisting of arrays of parallel pore channels with either 50, 100, or 200 nm diameters were used. For growth in PC templates, the PC membrane and the working electrode (aluminum) in a polypropylene filter holder were held in place with a silicone gasket. This assembly contacts the sol. The Pt counter electrode was also placed in the sol, parallel to the working electrode. Growth in AAM templates involved attaching the membrane to a working electrode, which was held parallel to the Pt counter electrode in a bath of the sol. The electric fields applied for the growth of nanorod arrays varied in the range of 0–6 V/cm. Detailed set-up can be found in our previous publications [7, 10–12]. After the growth of nanorod arrays, the filled templates were dried at 100°C for 24 hours and then fired at 500°C for 1 hour to densify and crystallize the grown nanorods. In the case of PC, the templates are removed upon firing at 500°C. For the removal of AAM templates, wet-chemical etching in 40% sodium hydroxide (NaOH) or potassium hydroxide (KOH) in water is required.

Details of zeta potential measurements and spectrometry analyses will be presented when discussing the relevant results. The resulting nanorod arrays after the removal of the templates were characterized by means of X-ray diffraction (XRD), scanning electron microscopy (SEM, JSM 5200), and transmission electron microscopy (TEM, EM420T).

3. Results and Discussion

3.1. Growth of Nanorods

Figure 2 shows typical SEM images of TiO_2 nanorods grown in PC membranes. The size of the nanorods is dependent on the pore size of the templates. Nanorods grown in 200, 100 and 50 nm templates pores resulted in nanorods with 180, 90 and 45 nm diameters, respectively. Figure 3 shows typical SEM images of TiO_2 nanorods grown in AAM with 200 nm pores. Both templates are very convenient to use for the growth of nanorod arrays by electrophoretic deposition, and each offers some advantages and disadvantages. The advantage of using PC as the template is its easy handling and easy removal by means of pyrolysis at elevated temperatures, but the flexibility and large thermal expansion coefficient of PC are prone to distortion and breakage of nanorods during the subsequent heat treatment and removal of the template. The advantage of using AAM as the template is its rigidity and resistance to high temperatures, allowing the nanorods to densify completely before removal. This would result in a large surface area of fairly free-standing and unidirectionally-aligned nanorod arrays. In addition, the AAM templates consist of a much higher pore density, and thus allow for the growth of a higher density of nanorods. The rigidity is also important for the attachment of nanorods to desired substrates. Furthermore, the thickness of AAM templates is typically 100 μm, 10 times that of the PC membranes. However, AAM
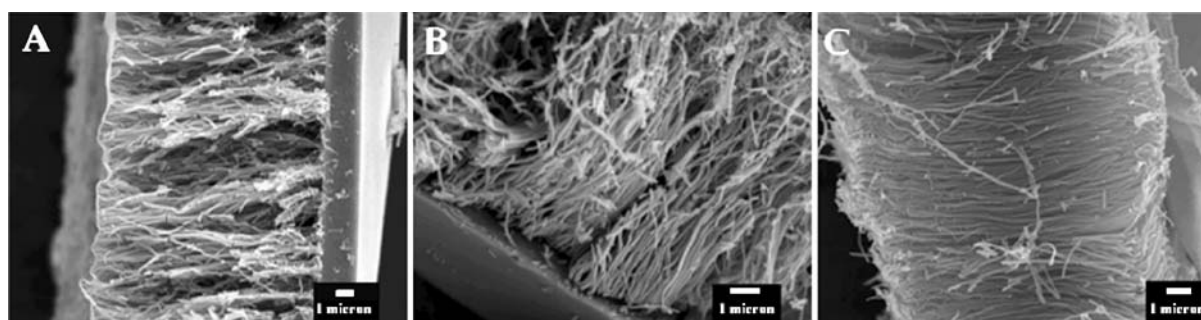
Figure 2. TiO_2 nanorods grown in PC templates with (a) 200 nm, (b) 100 nm and (c) 50 nm pores.
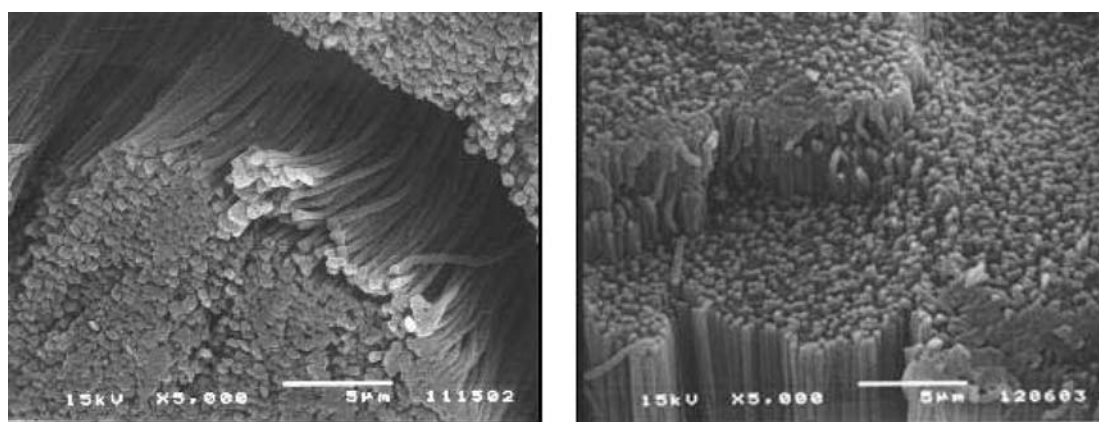
Figure 3. SEM images of TiO$_2$ nanorods grown in AAM, showing an array of nanorods (left) and nanorod arrays partially embedded in the template (right).

templates are very brittle and are easily broken during routine handling. In addition, wet-chemical etching seems to be the only method to remove the AAM templates and finding appropriate chemicals and etching parameters to dissolve the AAM templates without etching grown nanorods at the same time has proven to be challenging. Even with appropriate chemicals and etching parameters, it is difficult to remove AAM templates completely after nanorod growth, which hinders the practical applications of grown nanorod arrays.

3.2. Zeta Potential

Both sol particles and the template surface will develop a surface charge when in contact with a polar solvent. It is possible that the sign and magnitude of the particle and template surface charges could have an influence on the growth of the oxide nanorods. Table 1 lists the approximate zeta potentials for a number of the sols used in this work. Table 2 lists the approximate zeta potentials for two types of membranes (200 nm PC, and AAM), each in three different sols. Since it was difficult to directly measure the zeta potential of such small particles, the values in Table 1 were indirectly determined. The particle zeta potentials were difficult to obtain in parent sols; therefore, qualitative values were obtained by suspending sol powders in aqueous solutions with similar pH and ionic strength to the parent sol. The values in Table 2 were measured by chopping/crushing the membranes and dispersing them in the sols, then observing the velocities of the membrane particles under an applied field with an optical microscope. Strictly speaking, this method measured the zeta potential of the outside surface of the membrane, not that of the pore walls, which requires streaming potential measurements.

Although the particle zeta potential values are unlikely to be exactly equal to the zeta potentials of the sol nanoclusters, they are close enough to give good qualitative information about the behavior of the sols. From the Hückel equation, one can see that the mobility is directly proportional to the solution dielectric constant, and inversely proportional to the viscosity [13]:

$$\mu = \frac{2\varepsilon_r \varepsilon_0 \zeta}{3\pi\eta} \qquad (1)$$

In this equation, μ is the mobility (in m^{2}s^{-1} V^{-1}), ε_r is the dielectric constant of the fluid (no unit), ε_0 is the permittivity of vacuum, 8.845×10^{-12} F/m, ζ is the zeta potential (in V), and η is the fluid viscosity (in Pa-s). Based on the equation, both the dielectric constant and the viscosity have an influence on the mobility, but it was found that the particle zeta potential in aqueous media is a reasonable approximation. For instance, if one compares zeta potential data for PZT

Table 1. Zeta potentials of selected sols.

Sol	Measured zeta potential (mV)	pH
SiO$_2$	−8.14	3.05
TiO$_2$	18.85	2.07
PZT	7.63	4.08

Table 2. Measured template zeta potentials.

Membrane	Zeta pontential (m V) at pH = 2.0	Zeta potential (mV) at pH = 3.0	Zeta potential (mV) at pH = 4.0
PC	21.90	17.74	−7.12
AAM	33.70	28.57	16.61

in both aqueous [14] and ethanol [15] suspensions, the same general trend is observed. In both cases, the IEP is at ∼6.5–7, and the zeta potentials differ by less than 20% for most of the pH range. Thus, while the measured zeta potentials may not exactly coincide with the actual values, they are likely close enough, and follow the same trends, to give very useful information.

Furthermore, in the case of the template zeta potential, it is possible that values at the outside surface and within the pore walls differ. However, values obtained by streaming potential measurements of PC membranes, as shown in literature [16], are quite similar to values obtained by our method, at least for membranes with 100–200 nm pores. In addition, the data measured for AAM samples show reasonable agreement with reports from the literature [17] as well. The literature values are an average for AAM samples formed at several different current densities, in two different electrolytes. While these values did not exactly correlate with our measured data and our values differed from that reported in literature, AAM in both cases possessed positive zeta potential at pH values ranging from 2–5. Thus, the measured values for AAM zeta potential showed a reasonably close trend to the actual values. Similarly, the PC values were also quite close to those reported in the literature [16].

It has been reported by Wang et al. [18] suggesting that having a template surface charge of the same sign as the particle charge is necessary for the formation of solid nanorods over hollow nanotubes. Martin et al. [19] also observed the preferential formation of TiO_2 nanotubes under conditions where the TiO_2 particles are positively charged and the pore walls are assumed to be negatively charged. It is assumed that electrostatic attraction between the oppositely charged species leads to an initiation of gelation at the pore walls. This may explain some of the difficulties that have been experienced in synthesizing nanorods. The PC membranes used in synthesizing nanorods have their isoelectric point (IEP) at about pH ∼4 [20, 21], and thus have a positive surface charge at pHs below this value. Since all of the sols discussed above have pHs at or below 4, it is expected that growth will proceed as Wang et al proposed [18].

Attempts thus far to grow nanorods from sols with higher pHs have, however, been unsuccessful. Specifically, ZnO nanorods have been attempted from sols with pH's around 9. In these circumstances, the ZnO particles are positive (IEP of ZnO ∼9.3 [22]), but the PC pore walls are negative. A possible explanation for the failure to grow nanorods under these conditions is that electrostatic attraction between the ZnO particles and the pore walls caused the pore openings to become blocked, preventing nanorod growth. Two possible ways to overcome this are (1) to try increasing the voltage to overcome this attraction; or (2) to use a ZnO sol with a slightly higher pH, so that the ZnO particles will also be negatively charged. This also does not account for the ability to grow SiO_2 nanorods, since the particles in that sol are negatively charged.

Figure 4 shows SEM micrographs of SiO_2 nanorods grown in 200 nm PC templates with the working electrode as either the cathode or the anode, or with no applied voltage at all. It can be seen that placing the template on the anode led to the formation of solid nanorods. This is understandable, as the SiO_2 particles are negatively charged at the pH used. When the template was placed in the sol without an applied voltage, hollow SiO_2 nanotubes were formed. This is likely from the electrostatic attraction between the negative SiO_2 particles and the positively charged pore walls, similar to the TiO_2 nanotubes seen by Martin et al. [19]. Lastly, if the template was placed on the cathode, hollow tubes were seen, similar to those without an applied voltage. This is somewhat surprising, as it was expected that the negative sol particles would move away from the cathode under an applied voltage. Although these two samples appeared identical in cross-section, when viewed along their length, it was observed that those grown without an applied voltage were longer and more regular than those grown at the cathode.

In most cases, the templates used have a positive surface charge, except for the growth of PZT in PC, as
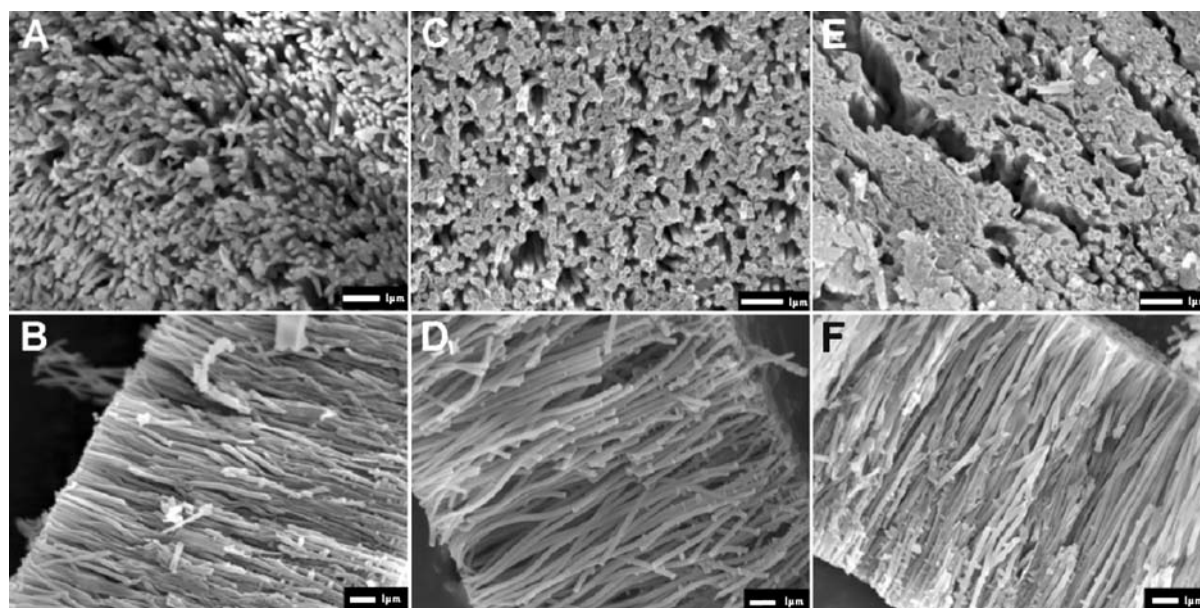
Figure 4. SiO$_2$ nanorods grown at the anode (A) and (B), without applied voltage (C) and (D), and at the cathode (E) and (F). The nanorods grown at the anode are solid, while the other two are hollow. All samples were grown for 1 hr in 200 nm templates.

shown in Table 2. This means that there would be an electrostatic repulsion between the positively charged nanoparticles and the pore walls, which should aid the formation of solid nanorods. For SiO$_2$, on the other hand, the nanoparticles are negatively charged and attracted to the pore walls, explaining the hollow rods observed when no electric field was applied. When the appropriate field was applied, however, solid rods were obtained in both SiO$_2$ and PZT, showing the effectiveness of EPD for the formation of dense deposits.

3.3. Deposition Rate

The influence of an electric field on deposition, for example, can be seen in the growth of PZT nanorods in 50 nm PC templates, as shown in Fig. 5. When the rods were grown with 5 V applied voltage, the nanorods formed were continuous (Fig. 5(a)). Upon increasing the voltage to 7 V, the nanorods were no longer solid (Fig. 5(b)), but strings of small, spherical particles.

In general, for the growth of oxide nanorods by electrophoresis, it is expected that the applied voltage for growth would have a significant influence on the product synthesized. Remembering that mobility equals velocity per unit field, the particle velocity can be expressed in terms of the charge on the nanoparticle and the applied electric field [13]:

$$v = \frac{qE}{6\pi \eta r} \qquad (2)$$

with E the electric field and v the velocity. According to Eq. (2), the velocity of the particles (and thus the deposition rate) is proportional to the electric field. Thus, at smaller applied voltages, slower growth rates are expected, and at higher voltages, the particles may be moving too quickly to form high-quality nanorods.

In addition, the separation by size of nanoparticles under the applied field could also influence the deposition and growth of the nanorods. If there is a distribution of nanoparticle sizes present in the sol, then there will be a distribution in the velocities of the particles, according to Eq. (2). This effect would become more pronounced at higher fields, leading to greater differences in deposition rate for small particles versus large particles.

There are three competing processes that can affect the quality of deposited nanorods: (1) the rate of arrival of nanoparticles at the growth surface, (2) the rearrangement of the particles to positions of lower free energy, and (3) the rate of condensation reactions between the particles (described in detail in the next section). As the moving nanoparticles arrive at the growth
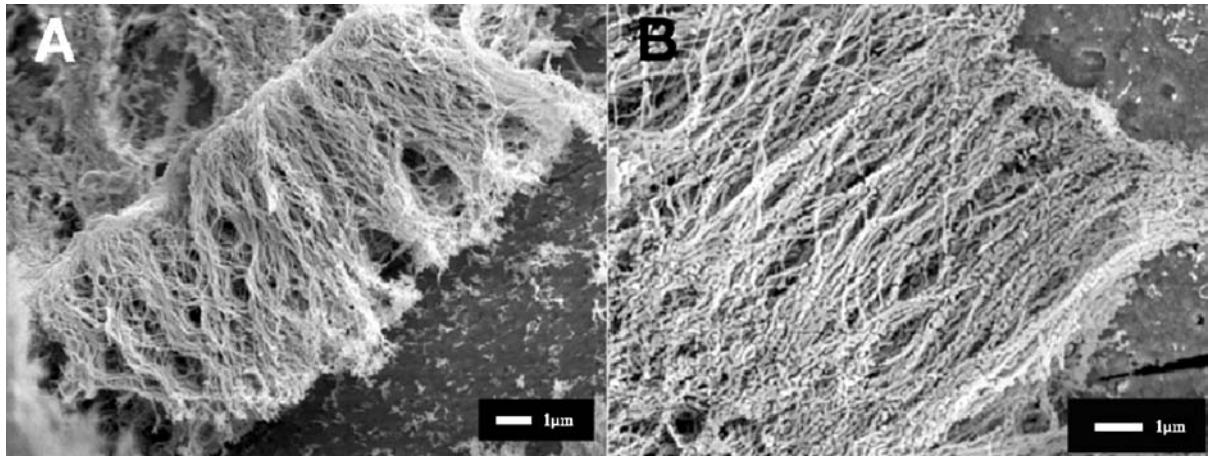
Figure 5. PZT nanorods grown at (A) lower and (B) higher voltages in 50 nm PC templates. At the higher voltage, the rods become discontinuous.

surface, they need some finite time to transport to a location of lower energy. If the applied field is too high, then the nanoparticles arrive at a faster rate than they re-arrange on the surface, causing them to become locked into position and reducing the quality of the deposit.

Further understanding of the effects of deposition rate on the density and quality of the nanorods came from analyzing samples of TiO_2 formed at a number of field strengths. As demonstrated in Fig. 6, the size of the sintered nanorods seemed to increase slightly with increasing deposition field, but overall, there was no no-

ticeable change and the variation in size was slight for growth in both the 100 and 200 nm templates. However, the quality of the rods varied. For TiO_2 rods formed at 1.84 V/cm in 100 nm templates, the result was a mat of short broken rods, rather than the nice parallel ar-ray seen at higher fields. This same behavior occurred in 200 nm templates without EPD and at a field of 0.17 V/cm. Additionally, the yield of rods under no applied field was very low. Thus, we find that if the deposition rate is slow with respect to the condensa-tion rate, then increasing the field increases the deposit
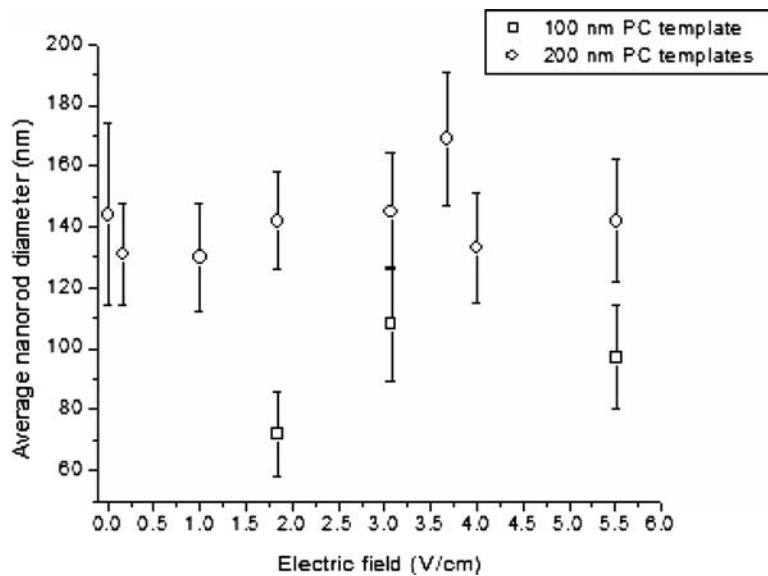
Figure 6. TiO_2 nanorod diameter vs. electric field used in electrophoretic deposition.

density. However, if the deposition is faster than the condensation rate, a less dense deposit is expected.

3.4.   Condensation Rate

When sol particles come within close contact, there are two important forces to consider. First, there is a van der Waals attraction between the two particles, holding them in close proximity. This attraction only holds the two particles in physical contact; it does not prevent re-arrangement of the relative positions of the two particles. Thus, even after two particles touch, they may still be able to re-arrange their relative positions to minimize the free energy of the system. Secondly, there is the possibility of condensation reactions occurring between the two nanoclusters. As exposed ─OH groups on the nanocluster surfaces come in contact, these reactions will generate covalent bonds between the two nanoparticles, locking them in place. The rate of these condensation reactions is an important consideration in the synthesis of nanorods. It is necessary to have enough condensation to hold the shape of the nanorods, but a slow enough rate that the particles can re-arrange themselves rather than just sticking wherever they deposit.

In order to observe the effects of condensation rate on the synthesis of nanorods, TiO_2 sols were prepared with a variety of pHs. First, TiO_2 sol was synthesized as

discussed previously. After the stable sol was formed, the pH was adjusted by the addition of concentrated nitric acid. This was done after a stable sol was formed, to have a minimal impact on the hydrolysis and formation of initial nanoparticles. To demonstrate the effect that pH adjustments have on the sols, and since gelation time is a good indicator of the condensation rate, gelation times were measured for a number of pHs. Figure 7 shows the approximate gelation time of the TiO_2 sols as a function of the pH. From this, it can be seen that the gelation kinetics are clearly influenced by the sol pH, especially at very low pH values. TiO_2 nanorods were synthesized from sols with varying pH, as described above. Figure 8 shows samples of TiO_2 rods grown from sols with a pH of 0.3 and 1.67 in 100 nm PC templates. The nanorods grown from the sol with pH = 0.3 have a much rougher surface morphology, and a large number of broken rods. This could be explained by the higher condensation rate in sols with higher acidity, as very well documented in silica sol [23, 24]. As the depositing nanoparticles arrive at the growth surface, a faster condensation rate causes the particles to be incorporated into the deposit much more quickly, without time to rearrange into a more favorable position. This could cause greater variations in the morphology, and lead to pores that would cause the rods to crack upon firing. However, the influence of pH is not strictly limited to effects on condensation rate. The sol pH also changes the zeta potential of the sol
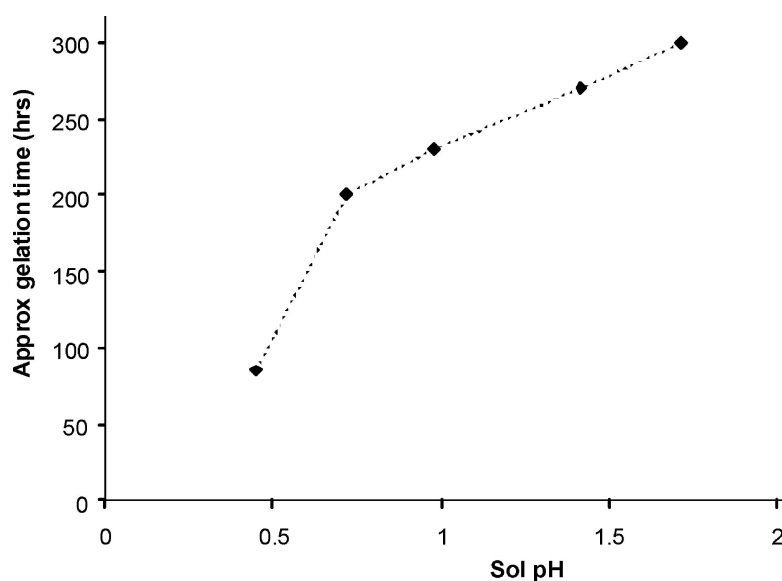
Figure 7.   Gelation time vs. sol pH for TiO_2 sols.
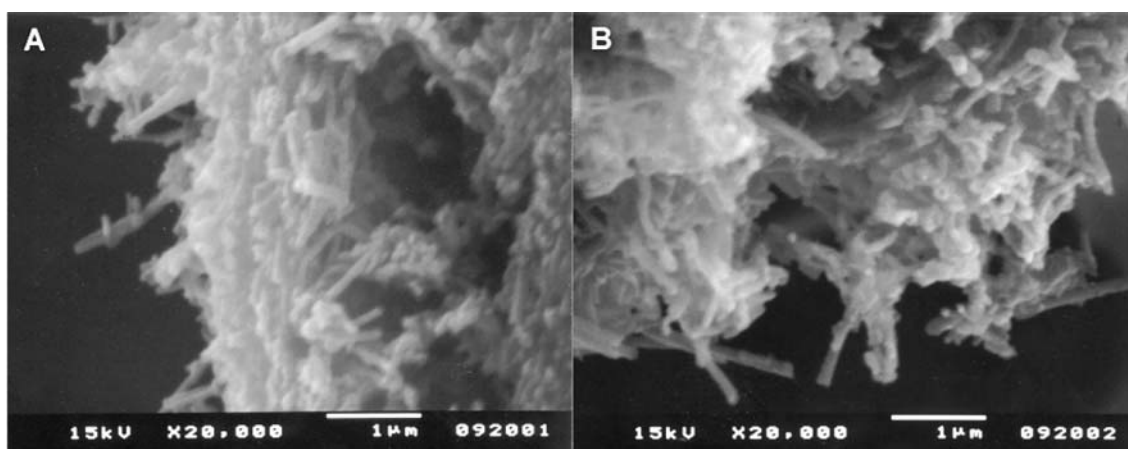
Figure 8. TiO$_2$ nanorods grown in 100 nm PC templates with AcAc added to the sol (A) before and (B) after hydrolysis.

nanoparticles, and thus their mobility. That is, lowering pH leads to an increase in both deposition rate and condensation rate. Since the relative strength of these two factors is not known for this sol, it is difficult to say with certainty which factor of this combined influence dominates. It is important to note that the use of partially nonaqueous sols could cause pH measurement errors of about 10–20%

3.5. Chemical Additives

The use of various organic additives to increase the stability of sols is well known, and these types of additives have become ubiquitous in sol preparation. In general, they work by binding to the precursors or nanoclusters in such a way as to slow down or prevent condensation reactions [25]. This is highly advantageous, and leads to the ability, for instance, to form stable sols even from highly reactive precursors. An example is the use of glacial acetic acid to stabilize TiO$_2$ sols. Direct addition of water to titanium alkoxides generally forms precipitates, but the use of acetic acid in this system leads to stable sols [26].

Table 3 shows a number of the sol compositions that failed to succeed in forming nanorods, along with the possible reasons. In contrast, Table 4 shows all the sol compositions that were used to successfully form nanorods. By comparison, it can be seen that the addition of 2,4-pentanedione (also known as acetylacetone, or AcAc) may have been the reason for no nanorod growth. AcAc is a very common additive in sol processing, and has long been used to prevent precipitation of

undesired phases from highly reactive precursors [27], to control crystal structure [28], and to aid in the formation of single-phase complex oxides [29]. It is quite likely that the use of AcAc is responsible for unsuccessful nanorod growth. It is widely known that AcAc binds strongly to a number of sol-gel precursors, such as Ti(OPr^i)$_4$ [23, 30] and Zr(OPr^n)$_4$ [31, 32], and is often incompletely hydrolyzed even in the presence of a large excess amount of water. This in turn inhibits condensation reactions and greatly slows the formation of a complete gel network. From Fig. 9, it can be seen that AcAc can inhibit nanorod formation. A sol that does yield nanorods (TiO$_2$) was modified by either adding

Table 3. Systems in which nanorods were not synthesized.

Sol	Observation	Possible reason (s)
Nb$_2$O$_5$ (1)	No rods	pH near IEP. Acetic acid
Nb$_2$O$_5$ (2)	No rods	Acetic acid
Nb$_2$O$_5$ (3)	No rods	Acetylacetone
V$_2$O$_5$	No rods	pH near IEP. Acetylacetone in some sols.
ITO	No rods	Acetylacetone is the main solvent
ZrO$_2$	Hollow (w and w/o EPD)	Uncertain
ZnO (1)	No rods	pH near IEP. DEA
ZnO (2)	No rods	Acetic acid
ZnO (3)	No rods	Uncertain, colloid pH well below IEP
WO$_3$ (1)	No rods	pH near IEP. Acetylacetone
WO$_3$ (2)	No rods	pH near IEP. Acetic acid

Table 4. Sol systems in which nanorods were successfully synthesized.

Sol	Precursors	Solvents/Other chemicals	Approx. pH
TiO_2	Titanium (IV) isopropoxide	Glacial acetic acid Water	~2
SiO_2	Tetraethyl orthosilicate	Ethanol Water Hydrochloric acid	~2
Nb_2O_5	Niobium chloride	Ethylene glycol Ethanol Water Citric acid	~1
V_2O_5	Vanadium pentoxide	Hydrogen peroxide Hydrochloric acid Water	~2.7
$Pb(Zr,Ti)O_3$	Lead acetate Titanium isopropoxide Zirconium *n*-propoxide	Glacial acetic acid Water Lactic acid Glycerol Ethylene glycol	~4
$BaTiO_3$	Titanium(IV) isopropoxide Barium acetate	Glacial acetic acid Ethylene glycol	~4 ~1
$SrNb_2O_6$	Strontium nitrate Niobium chloride	Ethylene glycol Ethanol Water Citric acid	
ITO	Indium chloride, Tin (IV) chloride	Ethylene glycol Ethanol Water Citric acid	~1
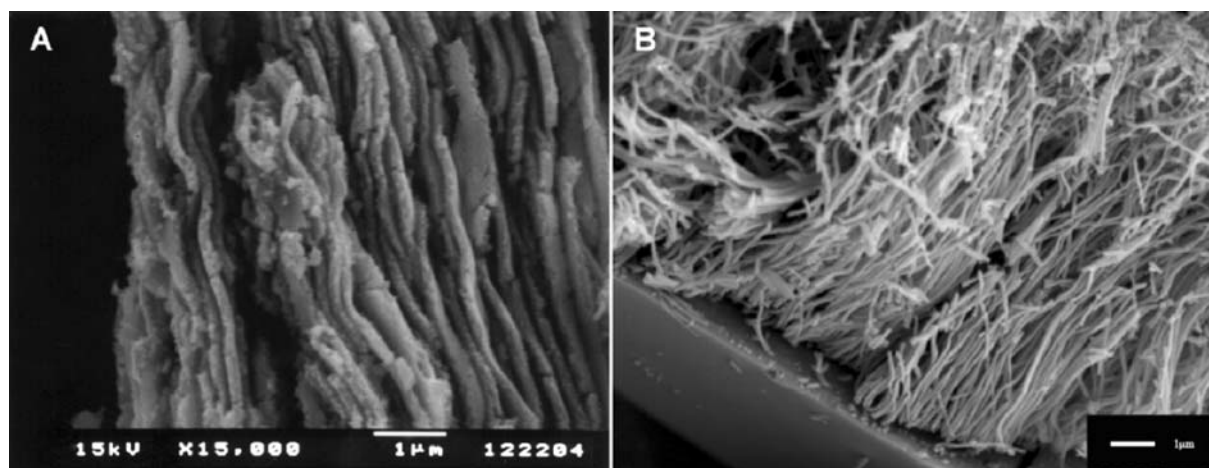
Figure 9. TiO_2 nanorods grown in 100 nm PC templates from sols with a pH of (A) 0.3 and (B) 1.67.

AcAc (in a ratio of Ti:AcAc = 1:1) before hydrolysis (TiO_2-AcAc1) or well after hydrolysis to the final stable sol (TiO_2-AcAc2). In both cases, only a few isolated shorter nanorods were observed, in contrast to the large arrays of nanorods seen when AcAc is omitted (as in Fig. 2).

Results from UV-vis absorbance spectra also give information about the effect of AcAc in TiO_2 sol.
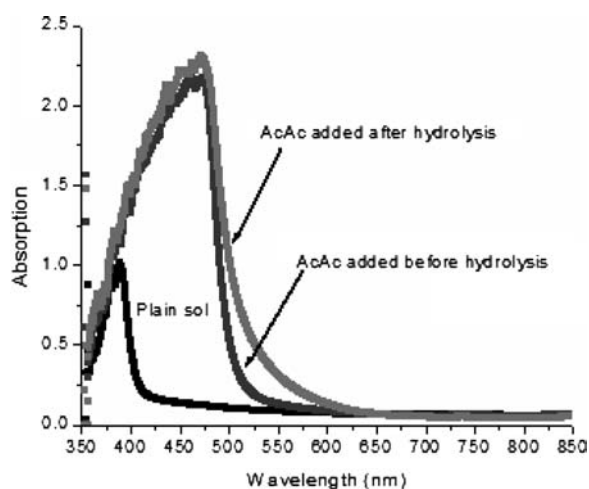
Figure 10.   UV-Vis absorbance of plain and AcAc-modified TiO$_2$ sols.

Figure 10 shows the absorption spectra of both the standard TiO$_2$ sol, along with the two different AcAc-modified sols (TiO$_2$-AcAc1 and TiO$_2$-AcAc2). In the standard sol, there is an absorbance peak at about ∼388 nm, likely due to the band-gap of the semi-crystalline TiO$_2$ nanoparticles in the sol. In AcAc-modified sols, however, there is a strong absorbance band in the visible, at about ∼475 nm. It is known that transition metals chelated with AcAc typically show a strong visible or

UV absorbance peak. Depending on the solvent and the exact ion chelated, the absorbance maximum can be anywhere from ∼240–810 nm [33–35]. Thus, the AcAc remains strongly bound to the Ti species, even after hydrolysis. Figure 11 also shows that AcAc is not fully hydrolyzed. The FTIR spectrum recorded for sol TiO$_2$—AcAc1 shows peaks at 1590 (v(C—O)) and 1534 (v(C—C)) cm^{-1} that are indicative of metal-AcAc complexes [36]. In addition to AcAc, the addition of glacial acetic acid and diethanolamine (DEA) in some cases also failed to yield nanorods, but is dependent on the relative strength of the metal-acetate bond, with some metals having relatively stronger bonding, and thus decreased condensation rates.

It is also important to note that the sol concentration does not appear to have a significant effect on the deposit, allowing the synthesis of solid nanorods even from very dilute sols, such as suggested by Wang et al [37]. The use of TiO$_2$ sols diluted with acetic acid after hydrolysis showed no difference in comparison with undiluted sols, as shown in Fig. 12. The SEM micrograph of TiO$_2$ nanorods grown in a 200 nm template at 1.67 V/cm from a dilute sol (0.17 vs. 0.85 M for the standard sol) shows that there is no significant difference between these rods and ones grown from the standard sol under similar conditions. The morphology of this sample is similar to what was observed in other cases, and the average diameter is in the same range as for the concentrated sol.
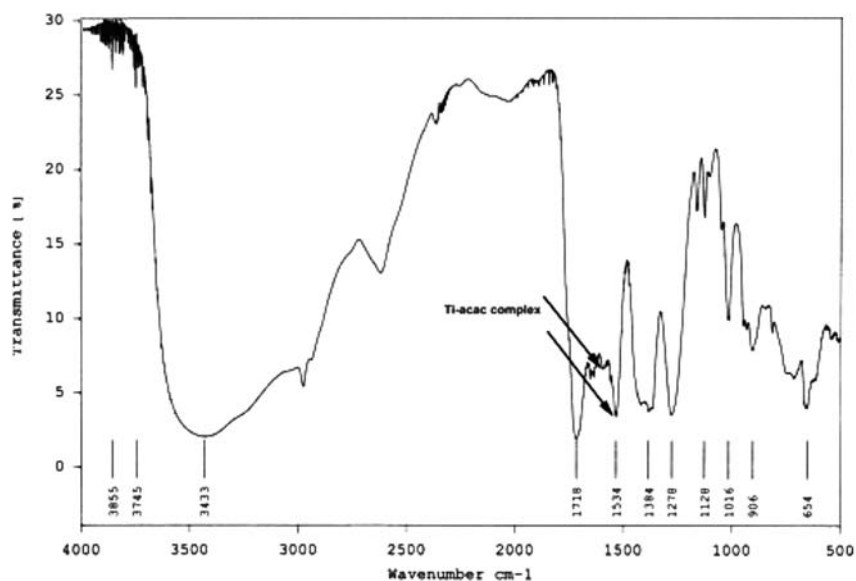
Figure 11.   FTIR spectra of TiO$_2$-AcAc1 sol.
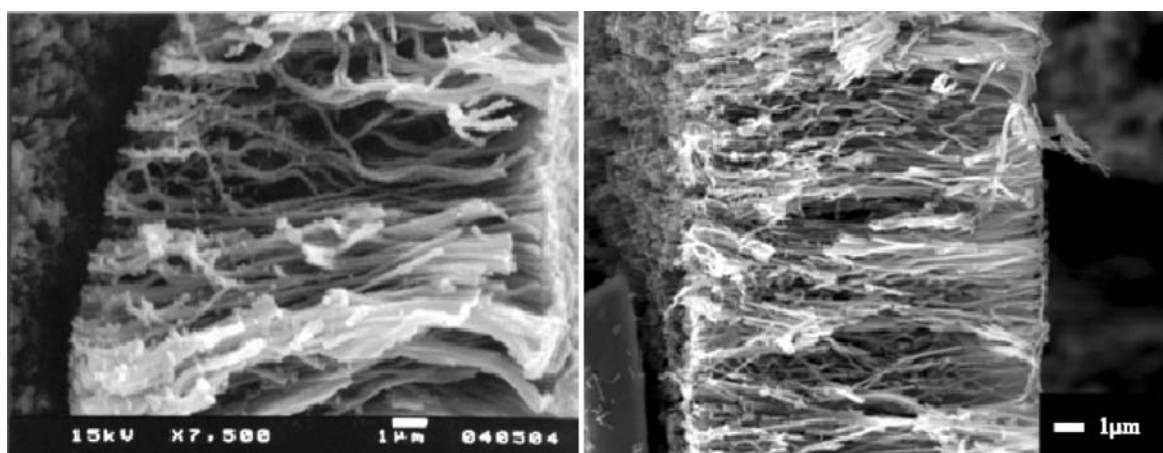
Figure 12. TiO$_2$ nanorods grown in 200 nm PC templates at 1.67 V/cm from 0.17 M (left) and 0.85 M (right) sols.

4. Conclusions

Among the parameters studied, zeta potential, external electric field, and organic additives appear to exert significant impact on the growth processes. Both higher zeta potential and externally applied electric field resulted in a higher growth rate, leading to relatively less dense packing. Less densely packed nanoclusters led to low green density and weak mechanical integrity; such nanorod arrays would either undergo substantial shrinkage with unacceptable distortion and non-uniformity, or would fall apart completely when subjected to firing during template removal. The signs of the particle zeta potential relative to that of the pores were found to be important. Templates with charge of opposite sign from that of the particles resulted in hollow nanotubes if the electrostatic attraction between the pore walls and the sol nanoparticles were stronger than the externally applied electric field. In addition, the presence of large organic molecules, particularly when they attach to the nanoclusters, shield the nanoparticles from the externally applied electric field, significantly undermining the electrophoretic motion and prevent adjacent nanoparticles from forming chemical bonds through surface condensation. A low surface condensation process would also permit the nanoparticles enriched and stacked on the growth surface to adjust their positions so that close packing can be achieved. Lastly, the sol concentration does not appear to have a significant effect on the deposit, allowing one to synthesize solid nanorods even from very dilute sols. Therefore, it is essential that appropriate parameters are used to successfully grow nanorod arrays by template-based sol electrophoresis.

References

1. G.Z. Cao, *Nanostructures and Nanomaterials: Synthesis, Properties, and Applications* (Imperial College Press, London, 2004).
2. C.M. Lieber, Solid State Comm. **107**, 607 (1998).
3. Y. Xia, P. Yang, Y. Sun, B. Wu, B. Mayers, B. Gates, Y. Yin, F. Kim, and H. Yan, Adv. Mater. **15**, 353 (2003).
4. G.R. Patzke, F. Krumeich, and R. Nesper, Angew. Chem. Int. Ed. **41**, 2447 (2002).
5. G.Z. Cao, J. Phys. Chem. **B108**, 19921 (2004).
6. Y. Lin, G.S. Wu, X.Y. Yuan, T. Xie, and L.D. Zhang, J Phys.-Condens. Mat. **15**, 2917 (2003).
7. S.J. Limmer, S.V. Cruz, and G.Z. Cao, Appl. Phys. **A79**, 421 (2004).
8. K. Takahashi, S.J. Limmer, Y. Wang, and G.Z. Cao, Jpn. J. Appl. Phys. **44B**, 662 (2005).
9. S.J. Limmer and G.Z. Cao, Adv. Mater. **15**, 427 (2003).
10. S.J. Limmer, S. Seraji, M.J. Forbess, Y. Wu, T.P. Chou, C. Nguyen, and G.Z. Cao, Adv. Mater. **13**, 1269 (2001).
11. S.J. Limmer, S. Seraji, Y. Wu, T.P. Chou, C. Nguyen, and G.Z. Cao, Adv. Funct. Mater. **12**, 59 (2002).

12. S.J. Limmer, T.P. Chou, and G.Z. Cao, J. Mater. Sci. **39**, 895 (2004).
13. R.J. Hunter, *Zeta Potential in Colloid Science* (Academic Press, London, 1981).
14. A. Navarro, J.R. Alcock, and R.W. Whatmore, J. Eur. Ceram. Soc. **24**, 1073 (2004).
15. J. Ma, R. Zhang, C.H. Liang, and L. Weng, Mater. Lett. **57**, 4648 (2003).
16. C. Lettmann, D. Möckel, and E. Staude, J. Membrane Sci. **159**, 243 (1999).
17. K.S. Seshadri, R. Kesavamoorthy, M.P. Srinivasan, K. Varatharajan, J. Ahmed, and V. Krishnasamy, B. Electrochem. **14**, 16 (1998).
18. Y.C. Wang, I.C. Leu, and M.H. Hon, J. Mater. Chem. **12**, 2439 (2002).
19. B.B. Lakshmi, P.K. Dorhout, and C.R. Martin, Chem. Mater. **9**, 857 (1997).
20. K.J. Kim, A.G. Fane, M. Nyström, and A. Pihlajamaki, J. Membrane Sci. **134**, 199 (1997).
21. C. Lettmann, D. Möckel, and E. Staude, J. Membrane Sci. **159**, 243 (1999).
22. M. Kosmulski, Langmuir **13**, 6315 (1997).
23. C.J. Brinker and G.W. Scherer, *Sol-Gel Science: The Physical and Chemistry of Sol-Gel Processing* (Academic Press, Boston, 1990).
24. R.K. Iler, *The Chemistry of Silica: Solubility, Polymerization, Colloid and Surface Properties, and Biochemistry* (John Wiley & Sons, New York, NY, 1979).
25. C. Sanchez, J. Livage, M. Henry, and F. Babonneau, J. Non-Cryst. Solids **100**, 65 (1988).
26. S. Barboux-Doeuff and C. Sanchez, Mat. Res. Bull. **29**, 1 (1994).
27. R. Nass and H. Schmidt, J. Non-Cryst. Solids **121**, 329 (1990).
28. T. Nishide and F. Mizukami, Thin Solid Films **259**, 212 (1995).
29. N. Tohge, E. Fujii, and T. Minami, J. Mater. Sci.-Mater. El. **5**, 356 (1994).
30. A. Leaustic, F. Babonneau, and J. Livage, Chem. Mater. **1**, 248 (1989).
31. P. Papet, N. Le Bars, J.F. Baumard, A. Lecomte, and A. Dauger, J. Mater. Sci. **24**, 3850 (1989).
32. M. Sedlar and M. Sayer, J. Sol-Gel Sci. Tech. **5**, 27 (1995).
33. S. Basu and K.K. Chatterji, Z. Phys. Chem. (Leipzig) **209**, 360 (1958).
34. K. Yamasaki, K. Sone, Nature **166**, 998 (1950).
35. J. Selbin, Chem. Rev. **65**, 153 (1965).
36. K. Nakamoto, *Infrared and Raman Spectra of Inorganic and Coordination Compounds*, 3rd (ed.) (John Wiley & Sons, New York, 1978).
37. Y.-C. Wang, I.-C. Leu, and M.-H. Hon, Electrochem. Solid St. **5**, C53 (2002).